Clues for a relation between rotational effects induced by the M_w6.3 2009 L'Aquila (Central Italy) earthquake and site and source effects

Luigi Cucci and Andrea Tertulliani

Istituto Nazionale di Geofisica e Vulcanologia

Corresponding author: Luigi Cucci, via di Vigna Murata 605 – 00143 Rome, Italy.

luigi.cucci@ingv.it

ABSTRACT

The M_w6.3 2009 L'Aquila earthquake produced an impressive number of rotational effects on vertically organized objects such as chimneys, pillars, capitals and gravestones. We present the dataset of such effects, that consists of 105 observations at 37 different sites and represents a compendium of earthquake-induced istances of rotational effects that is unprecedented in recent times. We find that the absolute majority of the reported effects was observed in the epicentral zone and that most of the observations are located where the MCS intensity is between 7 and 8-9. The evident asymmetry in the distribution of the rotational effects resembles the south-eastward directivity of the macroseismic effects and highlights a significant convergence between rotations and damage. Finally, we perform some qualitative analyses to recognize and evaluate which

geological and seismological parameters can be significant contributors to local rotations. We find that surface geology and amplification of the seismic motion at each reported location strongly influence the occurrence and the nature of the earthquake-induced rotational effects. Conversely, the contribution of the pattern of slip distribution on the fault plane plays only a secondary role in enhancing the rotational motion at each site.

INTRODUCTION

Rotational ground motion has long been ignored due to a widespread belief that rotation is not much significant (Gutenberg, 1927; Richter, 1958) and also to the difficulties experienced in measuring the small amplitudes of rotational motions. As a consequence, the studies on rotational effects from earthquakes have been progressively left aside with the advent of the fast-evolving, translational ground motion-oriented instrumental seismology. Nonetheless, earthquake-induced rotational effects have been known and were widely reported for centuries, as testified by a rotational component of the damage suffered by the blocks of the Marcus Aurelius' column of the Roman Imperial Age (Boschi et al., 1995).

The first significant historical instances of earthquake-induced rotational effects are provided by two Italian earthquakes, the M~7 1783 Calabria event and the M~7 1857 Great Neapolitan Earthquake, both occurred in the southern part of the Peninsula. In the aftermath of the 1783 earthquake, a scientific commission was appointed for the first time with the aim of reporting in detail the earthquake damage and other effects, paying particular attention to the pictorial rendering of the observations (Vivenzio 1783, 1788). However, no mechanical explanation of the observed effects was submitted till Mallet's early studies on this subject (Mallet 1848, 1849-50).

Following the 1857 earthquake, Mallet (1862) firstly formalized a number of mechanisms that satisfactorily explain the observed surface rotations, i.e. the rotation of bodies about their underlying structures. Such mechanisms derived from mechanical principles of seismic wave propagation and consisted in the mutual configuration of centre of gravity of a body, its friction with the base, and the horizontal component of seismic wave impact.

More recent studies, either based on direct observations or on numerical simulations, and reports about earthquake-induced rotational effects, underlined that rotational motions may be relevant in the near fault region of an earthquake. For example, Yamaguchi

and Odaka (1974) recorded important rotational effects of tombstones and stone lanterns caused by the M=6.9 Izu earthquake in 1974; Yegian et al (1994) found that following the M=6.8 1988 Armenia earthquake several grave markers in the Spitak's Cemetery rotated in a way as to be aligned with the direction of the main component of the horizontal motion.

In this paper we present the rotational effects associated to the 2009 L'Aquila earthquake, and perform qualitative analyses to recognize and evaluate what geological and seismological parameters can be significant contributors to local rotations. The aim of this paper is double, as on one hand we present a compendium of earthquake-induced istances of rotational effects that is unprecedented in recent times, and on the other hand our observations can be a spur for quantitative analyses of the data. For the description of our observations we adopt the notation proposed by Evans et al (2009) and the glossary by Lee (2009).

THE 2009 L'AQUILA EARTHQUAKE

The Abruzzi region of central Apennines experienced several destructive earthquakes in the last centuries (CPTI Working Group, 2009; Tertulliani et al., 2009), and is characterized by one of the

highest seismic hazards in Italy (Gruppo di Lavoro MPS, 2004; Pace et al., 2006; Akinci et al. 2009).

The 2009 earthquake hit during the night hours of April 6 a densely populated area of the Apennines (Figure 1) and was felt all over central Italy. The event occurred at about 9.5 km depth, and the epicentre was located few kilometers from the medieval town of L'Aquila (73.000 inhabitants at the time of the event). The April 6 earthquake was the peak of a four-month lasting sequence in which a total of >30.000 events were recorded, including two M5+ and several M4+ earthquakes occurred in the two weeks following the mainshock.

Although the M_w=6.3 magnitude of the event was not among the largest to have occurred in the Apennines, this earthquake can be considered as one of the most disastrous of the last 100 years, as it heavily affected the cultural and socio-economic fabric of a wide region characterized by high vulnerability. The shock caused the partial or total collapse of a significant number of highly vulnerable, historical buildings, provoking more than 300 casualties, thousands of injured, and leaving about sixty thousand homeless.

The seismicity distribution (Chiarabba et al., 2009), the focal mechanism of the mainshock (Pondrelli et al., 2009) and the GPS and DinSar modelling (Anzidei et al., 2009; Atzori et al., 2009;

Walters et al., 2009; Papanikolaou et al., 2010) concur to define a ~15 km-long, 50°SW-deep normal fault as the seismogenic source responsible of the event. The surface ruptures observed along the Paganica Fault (Figure 1) ~5 to ~10 km east of L'Aquila are located along the updip projection of the deep seismogenic source (Emergeo Working Group, 2010). The macroseismic survey of the 2009 seismic event showed that the largest damage was mainly distributed in a NW-SE direction and noticeably located SE of the instrumental epicenter (Galli et al., 2009), thus providing evidence of important directivity effects, confirmed by ground motion evidence (Cirella et al., 2009) and seismological analysis (Pino and Di Luccio, 2009).

MAP OF THE ROTATIONAL EFFECTS

During the macroseismic survey, performed in the aftermath of the 6 April mainshock in order to estimate the impact of the event, we collected a set of rotational effects on buildings, monuments in villages and cemeteries and heavy articles of furniture (Figure 2). The observations concern many manufactured objects retrieved rotated, in their entirety or partially, on the basement. In particular we observed the rotation of more than 50 chimneys, built in concrete blocks, bricks, or flues. The rotation can involve the body of the

chimney or the top only. Other typical objects were found investigating the cemeteries of the area, where tombstones, gravestones and other objects were rotated. In several occasions the rotation affected capitals or columns on walls or gates.

Our database counts 105 observations at 37 different sites (Figure 2 and Table 1) concentrated in the epicentral area. Each observation in Table 1 has been supplied with site coordinates, direction of rotations (clockwise or counter clockwise), quality factor (1 to 4, from clearly discernible rotation to discarded data), site intensity, site geology, and local amplification factor. The rotations are mainly concentrated in localities where the observed macroseismic intensity is within 7 and 8-9 (Galli et al., 2009). Also, the distribution of the rotational effects with respect to the epicenter shows a clear asymmetry (see rose diagram in Figure 2) that resembles the general pattern of damaging (Galli et al., 2009). In the town of L'Aquila we counted 23 rotated objects at 13 different sites, most of them located within the historical centre (Figure 3).

Though in the analysis of observed rotational effects it can be difficult to discriminate between true rotational motion and translational motion (e.g. Sargeant and Musson, 2009), in this paper we present only data that were assessed as due to actual rotational effects. Indeed the large number of observations is a demonstration

of how pervasive the phenomenon of rotations has been during this event.

ROLE OF SEISMOLOGICAL AND GEOLOGICAL PARAMETERS ON ROTATIONAL EFFECTS

Past studies have found that some seismological and geological factors can strongly influence and/or enhance the earthquake-induced rotational effects. As an example, Bouchon and Aki (1982) and Takeo and Ito (1997) found that large rotational velocities can be caused by rapid changes of slip on the fault plane or by heterogeneities of the rupture velocity, while Huang (2003) and Spudich and Fletcher (2008) claimed that local rheology and lateral geologic variations may play a crucial role in enhancing rotational velocities. Also, Stupazzini et al. (2009) found that peak ground rotation is strongly dependent on topographic, source and site effects.

Therefore, we performed qualitative analyses to evaluate possible correlations between our dataset and those seismological and geological factors. The latters, i.e. lithology and local amplification factor, are associated with the site of observation, whereas the seismological factors, i.e. the pattern of slip distribution on the fault plane, are associated with the earthquake source.

Rotations vs. geological factors

Peculiar geological conditions and/or potential amplification of the seismic shaking at a site can be considered factors that enhance the rotational motion. To assess whether the distribution of the observed rotations can be correlated with those geological factors, we superimpose our data on a geo-lithological map of the study area (Figure 4) based on the map by Vezzani and Ghisetti (1998) and integrated by detailed geological survey of the sites of observation. The map shows the limits between two main lithological units that are distinct on the base of their physical and geotechnical characteristics rather than their age or fossil content: R – rigid terrains (rigid and competent rocks like the outcrops of limestone and flysch bedrock); S – soft terrains (artificial landfills, fluvial and lacustrine deposits, alluvial fans, slope deposits, colluvia, fractured/weathered bedrock).

In Figure 4 we also show features from the map of the seismic microzonation of the study area (available at http://www.protezionecivile.it/cms/view.php?dir_pk=395&cms_pk=17356&n_page=1), which provides a characterization of the region in terms of seismic response, on the base of geomorphological observations and geophysical prospections. In our case we use in Figure 4 the final output of the microzonation map - the amplification

factor AF – a numeric parameter that describes how much the seismic signal at the site in study is amplified respect to a site of reference. The sites where rotational effects were observed have been divided in two classes, either stable sites with AF=1 (site not affected by amplification) or prone sites with AF>1 (site affected by amplification).

The results of the comparison between observed rotational motions and geological factors are shown in Table 2. Nineteen rotations out of 103 valid observations (18%) were observed on rigid lithologies, 84 were observed on soft lithologies (82%). As for the amplification factor, eighteen observations (17%) are associated to sites with AF=1, whereas 85 (83%) are associated to AF>1. A statistical check on all the remaining 33 sites that were located in the near fault region but where rotational effects did not occur, provides percentage rates clearly more balanced (Table 2) both between lithological units (R=61%, S=39%) and between seismic response (48% with AF=1, 52% with AF>1).

Furthermore, we divided our dataset of rotated objects into two other classes: free-field based (tombstones, gate pillars, etc.) and building based objects (chimneys, furniture, etc.). While free-field based objects can be considered as representative of pure rotational ground motion, building based objects could have been affected by

rotational modes of the underlying structure. The results displayed in Table 2 show that the rotations on building based objects are the absolute majority of the effects observed on stable sites and/or rigid lithologies, while the rotations on prone sites and/or soft lithologies almost equally distribute between free-field based and building based objects.

Rotations vs. seismological factors

Moderate magnitude earthquakes may evidence heterogeneities of the rupture on the fault and important directivity effects that can cause strong asymmetry of the damage distribution. At this stage we want to check for possible correlations between those seismological factors and our database of rotational effects.

Therefore, we superimpose our data on two different maps depicting the slip distribution along the earthquake source. In Figure 5a, the map from Cirella et al. (2010) images the rupture history of the L'Aquila earthquake using a nonlinear joint inversion of strong motion and GPS data, while in Figure 5b the map from Atzori et al (2009) shows the slip distribution inferred by the inversion of DInSAR coseismic displacement. Both these works agree in imaging a heterogeneous and complex rupture history, characterized by two main patches of slip. The largest slip concentration is located ~8 km SE of the nucleation, the second smaller slip patch is placed above

the hypocenter in the up-dip direction; maximum values of slip of ~1 m are reached along the main patch. Analyses of the source time function (Pino and Di Luccio, 2009), and of the coseismic and post-seismic slip from GPS data (Cheloni et al., 2010) confirm the rupture directivity toward the SE, in the direction of the largest slip patch.

We first compared the number of rotations that were observed on the seismogenic source to those observed off the fault. Then, we evaluated how many rotations were located within the zones of surface projection of the maximum slip. To this aim we took into account all the data falling within the slip contour of ≥ 0.4 m, which can be considered the threshold value to the largest slip concentration (S. Atzori, personal communication; cfr Wells and Coppersmith, 1994), and extends for about one third of the total fault area in the two maps of slip distribution.

Table 3 shows the results of the comparison between observed rotational motions and seismological factors. As for the Cirella et al's map, we found that 74 rotations (72% of the total) were located on the seismogenic source and 29 (28%) off the fault, while 30 rotations were observed in the area of largest slip (41% of the on-fault data, 29% of the total). The results from the Atzori et al's map are quite similar: 61 on-fault observations (59%), 42 off-fault (41%), and 29 on the largest slip zone (48% of the on-fault data, 28% of the total). In

the case of the Cirella et al's map, the check on the 33 'no data' sites that did not show rotational effects provides balanced results (Table 3) between the on-fault (54%) and off-fault (46%) sites, while the results in the area of largest slip are comparable to those of the rotational dataset (39% of the on-fault data, 21% of the total). The same check on the Atzori et al's map provides a higher percentage of off-fault data (70%) and less frequent observations in the largest slip zone (30% of the on-fault data, 9% of the total).

The results in Table 3 also show that the rotations of free-field based and building based objects affect the on-fault sites with quite similar occurrence, while the building based rotations become the great majority of the effects observed off the source. These results are noticeably comparable on both the maps of slip distribution.

DISCUSSION AND CONCLUSIONS

The analysis of our dataset provides a series of distinctive features:

- most of the rotational effects were detected on vertically organized objects such as chimneys, pillars, capitals and gravestones.
- number, variety and distribution of our data allow us to believe that the observed effects are due to actual rotational motion.

- the absolute majority of the reported effects were observed in the near field zone (98% within a distance of one fault-length) and in the epicentral zone (89% at a distance ≤15 km from the epicenter).

- most of the observations are located where the MCS intensity is between 7 and 8-9; only 22 out of 103 considered rotations (21%) are concentrated within the highest intensities (9-9.5) associated to the event.

- there are evident clues of directivity toward the South-East also in the distribution of the rotational effects. Indeed the rotations are observed along-strike up to 23 km from the epicenter SE-ward, and only up to 5 km from the epicenter NW-ward.

- from the above-mentioned points it stems that there is a significant convergence between rotations and damage, as the general distribution of the rotational effects clearly resembles that of the intensities.

Moreover, significant results are obtained from the comparison between the distribution of earthquake-induced rotational data and the seismological and geological factors that can influence them.

1) The comparison between observed data and geological factors clearly indicates that the rotational motion can be enhanced by the particular geological setting at a site. The absolute majority of the rotational effects (more than 80%) occurred where the site of

observation was affected by scarce geophysical and/or geotechnical characteristics, or by unfavorable geomorphological conditions. Such a large percentage becomes even more remarkable when compared to that associated to other localities with no rotational effects, equally distributed between geologically favorable and unfavorable sites. To this end, we want to point out that the different behaviour between the ‘data’ and the ‘no data’ points can not be ascribed to lower average epicentral distances, that actually are comparable (12 and 15 km, respectively).

2) The comparison between observed rotations and seismological factors provides contradictory, less convergent results. In fact, on one side there is the indication of a relation between the location of the data and the position of the seismogenic source, as most (about two thirds) of the observations fall within the surface projection of the Paganica fault plane. On the other side, when we restrict our analysis to the anomalies of the slip distribution, we observe that only less than 50% of the ‘on-fault’ rotations are also located within the areas of maximum slip. The relatively limited extension of the ≥ 0.4 m slip area respect to the total fault area only partially accounts for this evidence. In addition, also the ‘no data’ sites display a similar behaviour, as they show a slightly lower but similar proportion of localities situated in the maximum slip zones.

3) The rotational effects observed on free-field based and on building based objects are characterized by a different behaviour when they are put in relation with the geological and seismological features. Indeed there is the evidence that free-field based rotations occurred almost exclusively on soft terrains and/or on prone sites with AF>1 located on the seismogenic source. Therefore, while rotational modes of edifices can be observed on different settings of lithology and of amplification and become predominant away from the fault, pure ground motion rotation preferably affects sites located close to the epicenter and characterized by poor geophysical and geomorphological conditions.

In summary then, from the analysis of our data we can affirm that site effects, i.e. surface geology and amplification of the seismic motion at each reported site, strongly influence the occurrence and the nature of the earthquake-induced rotational effects. Conversely, the contribution of the source effects, i.e. the pattern of slip distribution on the fault plane, plays only a secondary role in enhancing the rotational motion at each site.

This kind of analyses can provide estimates of ground motions parameters and support important insights to the applications in earthquake engineering. We believe that this work can represent a valid reference for future investigations, in particular when a

moderate magnitude earthquake occurs in densely populated regions, as in the case of L'Aquila.

DATA AND RESOURCES

All data used in this paper were collected during field survey and are available by the authors.

ACKNOWLEDGEMENTS

We want to thanks C. Castellano for help during the field work and assistance in the preparation of the photographs, and Ina Cecic, Matjaz Godec and Tiziana Tuvé for providing several photos. Thanks are due to Francesca R. Cinti who read and corrected a first draft of the manuscript. M. Mucciarelli and an anonymous reviewer provided constructive suggestions and comments that greatly improved the paper.

REFERENCES

Akinci, A., Galadini, F., Pantosti, D., Petersen, M., Malagnini, L., and D. Perkins (2009). Effect of time dependence on probabilistic seismic-hazard maps and segregation for the central Apennines, Italy, *Bull. Seism. Soc. Am.* **99** 585-610.

Anzidei, M., Boschi, E., Cannelli, V., Devoti, R., Esposito, A., Galvani, A., Melini, D., Pietrantonio, G., Riguzzi F., Sepe, V., and E. Serpelloni (2009). Coseismic deformation of the destructive April 6, 2009 L'Aquila earthquake (central Italy) from GPS data, *Geophys. Res. Lett.* 36 L17307.

Atzori, S., Hunstad, I., Chini, M., Salvi, S., Tolomei, C., Bignami, C., Stramondo, S., Trasatti, E., Antonioli, A., and E. Boschi (2009). Finite fault inversion of DInSAR coseismic displacement of the 2009 L'Aquila earthquake (central Italy), *Geophys. Res. Lett.* **36** L15305.

Boschi, E., Caserta, A., Conti, C., Di Bona, M., Funiciello, R., Malagnini, L., Marra, F., Martines, G., Rovelli, A., and S. Salvi (1995). Resonance of subsurface sediments: an unforeseen

complication for designers of Roman columns, *Bull. Seism. Soc. Am.* **85** 320-324.

Bouchon, M., and K. Aki (1982). Strain, tilt, and rotation associated with strong ground motion in the vicinity of earthquake faults, *Bull. Seism. Soc. Am.* **72** 1717-1738.

Cheloni, D., D'Agostino N., D'Anastasio E., Avallone A., Mantenuto S., Giuliani R., Mattone M., Calcaterra S., Gambino P., Dominici D., Radicioni F., and G. Fastellini (2010). Coseismic and initial post-seismic slip of the 2009 Mw 6.3 L'Aquila earthquake, Italy, from GPS measurements, *Geophys. J. Int*. **181** 1539-1546.

Chiarabba, C., Amato, A., Anselmi, A., Baccheschi, P., Bianchi, I., Cattaneo, M., Cecere, G., Chiaraluce, L., Ciaccio, M.G., De Gori, P., De Luca, G., Di Bona, M., Di Stefano, R., Faenza, L., Govoni, A., Improta, L., Lucente, F.P., Marchetti, A., Margheriti, L., Mele, F., Michelini, A., Monachesi, G., Moretti, M., Pastori, M., Piana Agostinetti, N., Piccinini, D., Roselli, P., Seccia, D., and L. Valoroso (2009). The 2009 L'Aquila (central Italy) M_w6.3 earthquake: main shock and aftershocks, *Geophys. Res. Lett*. **36** L18308.

Cirella, A., Piatanesi, A., Cocco, M., Tinti, E., Scognamiglio, L., Michelini, A., Lomax, A., and E. Boschi (2009). Rupture history of the 2009 L'Aquila (Italy) earthquake from non-linear joint inversion of strong motion and GPS data, *Geophys. Res. Lett*. **36** L19304.

Cirella, A., Piatanesi, A., Tinti, E., Chini, M., and M. Cocco (2010). Source complexity of the 2009 L'Aquila, Italy, earthquake retrieved from the joint inversion of strong motion, GPS and DInSAR data – Evidence for a rheological control on rupture mechanics, *Geophysical Research Abstracts* **12** EGU2010-4983.

CPTI Working Group (2004). *Catalogo Parametrico dei Terremoti Italiani, versione 2004 (CPTI04),* INGV, Bologna, http://emidius.mi.ingv.it/CPTI04/.

Emergeo Working Group (2010). Evidence for surface rupture associated with the Mw 6.3 L'Aquila earthquake sequence of April 2009 (central Italy), *Terra Nova* **22** 43–51.

Evans, J.R., and International Working Group on Rotational Seismology (2009). Suggested notation conventions for rotational seismology, *Bull. Seism. Soc. Am.* **99** 1073-1075.

Galli, P., Camassi, R., Azzaro, R., Bernardini, F., Castenetto, S., Molin, D., Peronace, E., Rossi, A., Vecchi, M., and A. Tertulliani (2009). Terremoto de L'Aquila del 6 aprile 2009: distribuzione delle intensità macrosismiche ed implicazioni sismotettoniche, *Il Quaternario* **22** 235-246.

Gruppo di Lavoro MPS (2004). *Redazione della mappa di pericolosità sismica prevista dall'ordinanza PCM 3274 del 20 Marzo 2003.* Rapporto Conclusivo per il Dipartimento della Protezione Civile, INGV, Milano-Roma, aprile 2004, 65 pp + 5 appendici.

Gutenberg, B. (1927). *Grundlagen der Erdbebenkunde*, univ. Frankfurt a/M, 189 pp.

Huang, B.-S. (2003). Ground rotational motions of the 1999 Chi-Chi, Taiwan, earthquake as inferred from dense array observations, *Geophys. Res. Lett.* **30** 1307.

Lee, W.H.K. (2009). A glossary for rotational seismology, *Bull. Seism. Soc. Am.* **99** 1082-1090.

Mallet, R. (1848). Dynamics of earthquakes, *Trans. R. Irish Acad*. **XXI** 51.

Mallet, R. (1849-1850). On vorticose shock and case of twisting, in *Admiralty Manual*, Meeting Brit. Assoc., 33 and 49, 213 pp.

Mallet, R. (1862). *Great Neapolitan Earthquake of 1857: the first principles of observational seismology as developed in the Report to the Royal Society of London of the expedition made by command of the Society into the interior of the Kingdom of Naples to investigate the circumstances of the great earthquake of December 1857*, 2 Volumes, Chapman and Hall, London.

Pace, B., Peruzza, L., Lavecchia, G., and P. Boncio (2006). Layered seismogenic source model and probabilistic seismic-hazard analyses in central Italy, *Bull. Seism. Soc. Am.* **96** 107-132.

Papanikolaou, I.D., Foumelis, M., Parcharidis, I., Lekkas, E.L., and I.G. Fountoulis (2010). Deformation patern of the 6 and 7 April 2009, M_w=6.3 and M_w=5.6 earthquakes in L'Aquila (Central Italy) revealed by ground and space based observations, *Nat. Hazards Earth Syst. Sci.* **10** 73-87.

Pino, A., and F. Di Luccio (2009). Source complexity of the 6 April 2009 L'Aquila (central Italy) earthquake and its strongest aftershock revealed by elementary seismological analysis, *Geophys. Res. Lett.* **36** L23305.

Pondrelli, S., Salimbeni, S., Morelli, A., Ekström, G., Olivieri, M., and E. Boschi (2010). Seismic moment tensors of the April 2009, L'Aquila (Central Italy), earthquake sequence, *Geophys. J. Int*. **180** 238-242.

Richter, C.F. (1958). *Elementary seismology*, W.H. Freeman and Company, San Francisco, 129-132.

Sargeant, S.L., and R.M.W. Musson (2009). Rotational earthquake effects in the United Kingdom, *Bull. Seism. Soc. Am.* **99** 1475-1479.

Spudich, P., and J.B. Fletcher (2008). Observation and prediction of dynamic ground strains, tilts, and torsions caused by the M_w6.0 2004 Parkfiled, California, earthquake and aftershocks, derived from UPSAR array observations, *Bull. Seism. Soc. Am.* **98** 1898-1914.

Stupazzini, M., de la Puente, J., Smerzini, C., Käser, M., Igel, H., and A. Castellani (2009). Study of rotational ground motion in the near-field region, *Bull. Seism. Soc. Am.* **99** 1271-1286.

Takeo, M., and H.M. Ito (1997). What can be learned from rotational motions excited by earthquakes?, *Geophys. J. Int*. **129** 319-329..

Tertulliani, A., Rossi, A., Cucci, L., and M. Vecchi (2009). L'Aquila (Central Italy) earthquakes: the predecessors of the April 6, 2009 event, *Seismol. Res. Lett.* **80** 1008-1013.

Vezzani, L., and F. Ghisetti (1998). Carta Geologica dell'Abruzzo, scala 1:100.000, S.EL.CA., Firenze.

Vivenzio, G. (1783). *Istoria e teoria de' tremuoti in generale, ed in particulare di quelli della Calabria e di Messina del 1783*, Stamperia Reale, Napoli.

Vivenzio, G. (1788). *Istoria de' tremuoti avvenuti nella provincia della Calabria ulteriore e nella città di Messina nell'Anno 1783, e do quanto nella Calabria fu fatto per lo suo Risorgimento fino al 1787,*

preceduta da una teoria ed istoria generale de' tremuoti, Vol. 1-2, Stamperia Reale, Napoli.

Walters, R.J., Elliott, J.R., D'Agostino, N., England, P.C., Hunstad, I., Jackson, J.A., Parsons, B., Phillips, R.J., and G. Roberts (2009). The 2009 L'Aquila earthquake (central Italy): a source mechanism and implications for seismic hazard, *Geophys. Res. Lett*. **36** L17312.

Wells, D.L., and K.J. Coppersmith (1994). New empirical relationships among magnitude, rupture length, rupture width, rupture area, and surface displacement, *Bull. Seism. Soc. Am.* **84** 974-1002.

Yamaguchi , R., and T. Odaka (1974). Field study of the Izu-Hanto-oki earthquake of 1974, *Special Bull. Earthq. Res. Inst.,* Univ. Tokyo*,* **14***,* 241-255*.*

Yegian, M.K., Ghahraman, V.G., and G. Gazetas (1994). 1988 Armenia earthquake. II: damage statistics versus geologic and soil profiles, *Journal of Geotechnical Engineering* **120** 21-45.

FIGURE CAPTIONS

Figure 1 – Map of the study area. The focal mechanism by Pondrelli et al. (2009) indicates the position of the epicenter of the April 6, 2009 L'Aquila earthquake. Aftershock distribution from ISIDe, the Italian Seismic Instrumental and parametric Data-basE (http://iside.rm.ingv.it/iside/standard/index.jsp). A solid curved line encircles the area where earthquake-induced rotational effects have been observed. We also indicate the surface expression of the normal Paganica Fault (hachures on the hanging wall) and the main localities in the study area along with their MCS intensity (Galli et al., 2009).

Figure 2 – Map of the sites of observation of rotational effects and examples of rotations. The focal mechanism indicates the epicenter of the 2009 L'Aquila earthquake. The rose diagram shows the distribution of the azimuths between the rotation points and the epicenter (see also Table 1). The numbers in the lower right corner of each photo indicate the corresponding record in Table 1. A dashed rectangle indicates the area of Figure 3.

Figure 3 – Map of the rotational effects observed in the town of L'Aquila. The numbers inside the circles indicate multiple observations

associated to the same location. The numbers in the lower right corner of each photo indicate the corresponding record in Table 1.

Figure 4 – Rotational effects, lithology, and seismic microzonation in the study area. The geo-lithological map, simplified from Vezzani and Ghisetti (1998), reports two main classes of outcrops: 'R' – rigid rocks (mainly limestone and flysch bedrock), and 'S' – soft rocks (artificial landfills, fluvial and lacustrine deposits, alluvial fans, slope deposits, colluvia, fractured/weathered bedrock). Circles represent sites of observed rotations ranked by the local amplification factor AF (see http://www.protezionecivile.it/cms/view.php?dir_pk=395&cms_pk=17356 for further information): black circle – stable site, white circle – prone site. Due to velocity inversion, at some sites amplification can be associated to 'R' outcrops (e.g., cemented breccias overlying clays overlying limestones). Numbers in parenthesis indicate multiple observations associated to the same location. Crossed circles indicate sites where rotational effects did not occur. A black star shows the location of the epicenter of the L'Aquila earthquake.

Figure 5 - Rotational effects and slip distribution in the study area. Different colored areas represent the slip distribution on the fault plane. Black circles show the sites of observed rotations (numbers in

parenthesis indicate multiple observations associated to the same location). Crossed circles indicate sites where rotational effects did not occur. A black star shows the location of the epicenter of the L'Aquila earthquake. a) comparison with the map modified from Cirella et al. (2010); b) comparison with the map modified from Atzori et al. (2009).

Table

NO	LOCALITY	LAT	LON	AZIM	OBJECT	QF	REMARKS	MCS	BASE	AF	LIT
1	Aragno	42,396	13,459	57°	chimney	1	cw	6	bdg	1	R
2	Aragno (cemet.)	42,394	13,459	58°	tombstone	3	ccw	6	ffd	>1	S
3	Assergi	42,414	13,505	60°	chimney	1	ccw	6	bdg	>1	S
4	Barisciano	42,325	13,591	99°	chimney	1	cw	6	bdg	>1	S
5	Bazzano	42,337	13,453	98°	chimney	1	ccw	8	bdg	1	R
6	Bazzano	42,338	13,454	98°	chimney	1	cw	8	bdg	1	R
7	Camarda	42,39	13,494	67°	chimney	1	ccw	7,5	bdg	>1	R
8	Cansatessa	42,384	13,343	343°	furniture	1	ccw	6,5	bdg	>1	S
9	Casentino (cemet.)	42,28	13,514	122°	facade	1	ccw	8	bdg	>1	S
10	Casentino	42,279	13,511	124°	vase	1	cw	8	ffd	>1	S
11	Casentino	42,279	13,51	124°	chimney	1	cw	8	bdg	>1	S
12	Castel del Monte	42,325	13,727	90°	merlon	2	cw	6	bdg	1	R
13	Castelnuovo (cemet.)	42,298	13,624	105°	monument	1	ccw	9,5	ffd	>1	S
14	Castelnuovo (cemet.)	42,298	13,625	105°	pinnacle	1	ccw	9,5	ffd	>1	S
15	Civitella Casanova	42,364	13,889	91°	stone	4	cw	6	bdg	NA	S
16	Colle di Lucoli	42,308	13,334	206°	chimney	1	cw	7,5	bdg	1	R
17	Colle di Roio	42,342	13,349	229°	chimney	1	ccw	8	bdg	>1	R
18	Colle di Roio	42,342	13,349	229°	chimney	1	ccw	8	bdg	>1	R

19	Collimento	42,292	13,34	197°	chimney	2	ccw	6,5	bdg	1	R
20	Collimento	42,291	13,338	198°	statue	1	cw	6,5	ffd	1	R
21	Collimento	42,29	13,337	198°	chimney	1	cw	6,5	bdg	1	R
22	Coppito	42,368	13,341	326°	chimney	1	ccw	6,5	bdg	1	S
23	Coppito	42,368	13,341	326°	chimney	2	ccw	6,5	bdg	1	S
24	Filetto	42,378	13,52	77°	chimney	1	cw	6	bdg	1	R
25	Fossa (cemet.)	42,302	13,482	118°	vase	1	ccw	7,5	bdg	>1	S
26	Fossa (cemet.)	42,302	13,482	118°	pillar	1	ccw	7,5	ffd	>1	S
27	Fossa (cemet.)	42,302	13,482	118°	pillar	1	ccw	7,5	ffd	>1	S
28	Fossa	42,291	13,488	123°	chimney	2	ccw	7,5	bdg	>1	S
29	L’Aquila civico13	42,35	13,398	90°	capital	1	cw	8,5	ffd	>1	S
30	L’Aquila (cemet.)	42,351	13,412	89°	grave	1	ccw	8,5	ffd	>1	S
31	L’Aquila civico13	42,35	13,398	90°	capital	3	ccw	8,5	ffd	>1	S
32	L’Aquila civico13	42,35	13,398	90°	capital	3	cw	8,5	ffd	>1	S
33	L’Aquila corso	42,346	13,398	93°	marble cover	1	ccw	8,5	bdg	>1	S
34	L’Aquila Anime Sante	42,347	13,396	93°	chimney	1	ccw	8,5	bdg	>1	S
35	L’Aquila NW	42,35	13,395	88°	pillar	1	ccw	8,5	ffd	>1	S
36	L’Aquila west	42,359	13,363	9°	chimney	3	cw	8,5	bdg	>1	S
37	L’Aquila Porta Napoli	42,342	13,395	104°	capital	1	cw	8,5	ffd	>1	S

38	L’Aquila S. Maria a Paganica	42,353	13,4	82°	balustrade	1	ccw	8,5	bdg	>1	S
39	L’Aquila S. Maria Miseric.	42,354	13,398	81°	pillar	1	ccw	8,5	bdg	>1	S
40	L’Aquila S. Pietro Coppito	42,352	13,395	80°	marble stone	1	ccw	8,5	ffd	>1	S
41	L’Aquila S. Pietro Coppito	42,352	13,395	80°	marble stone	1	cw	8,5	ffd	>1	S
42	L’Aquila S. Pietro Coppito	42,352	13,395	80°	marble stone	1	cw	8,5	ffd	>1	S
43	L’Aquila S. Pietro Coppito	42,352	13,395	80°	marble stone	1	cw	8,5	ffd	>1	S
44	L’Aquila S. Pietro Coppito	42,352	13,395	80°	marble stone	1	cw	8,5	ffd	>1	S
45	L’Aquila S. Pietro Coppito	42,352	13,395	80°	marble stone	1	cw	8,5	ffd	>1	S
46	L’Aquila università	42,351	13,397	80°	pillar	1	cw	8,5	ffd	>1	S
47	L’Aquila università	42,351	13,397	80°	pillar	1	ccw	8,5	ffd	>1	S
48	L’Aquila università	42,351	13,397	80°	pillar	1	ccw	8,5	ffd	>1	S
49	L’Aquila via Bafile	42,352	13,398	79°	vase	1	ccw	8,5	bdg	>1	S
50	L’Aquila via della Genca	42,354	13,4	78°	statue	1	cw	8,5	bdg	>1	S
51	L’Aquila via XX settembre	42,348	13,392	91°	chimney	3	ccw	8,5	bdg	>1	S
52	L’Aquila via XX settembre	42,347	13,393	91°	chimney	1	ccw	8,5	bdg	>1	S
53	Monticchio (cemet.)	42,315	13,462	115°	pinnacle	1	cw	6	ffd	>1	S
54	Onna	42,327	13,481	104°	chimney	1	cw	9,5	bdg	>1	S
55	Onna	42,327	13,478	105°	pillar	3	cw	9,5	ffd	>1	S
56	Onna	42,331	13,468	102°	chimney	1	cw	9,5	bdg	>1	S

57	Paganica	42,362	13,467	83°	chimney	1	ccw	8	bdg	>1	S
58	Paganica	42,359	13,471	84°	monument	1	ccw	8	ffd	>1	S
59	Paganica	42,358	13,4705	84°	chimney	1	cw	8	bdg	>1	S
60	Paganica	42,358	13,471	84°	pinnacle	1	ccw	8	bdg	>1	S
61	Paganica	42,361	13,472	84°	vase	1	ccw	8	ffd	>1	S
62	Paganica	42,36	13,474	85°	chimney	1	cw	8	bdg	>1	S
63	Paganica	42,359	13,471	84°	chimney	1	ccw	8	bdg	>1	S
64	Paganica	42,365	13,469	80°	chimney	1	cw	8	bdg	>1	S
65	Pianola	42,322	13,404	127°	chimney	1	cw	7	bdg	1	R
66	Poggio di Roio	42,331	13,378	140°	chimney	3	ccw	8,5	bdg	1	R
67	Poggio Picenze	42,32	13,538	103°	chimney	1	cw	8,5	bdg	>1	S
68	Poggio Picenze	42,318	13,541	104°	chimney	2	cw	8,5	bdg	>1	S
69	Poggio Picenze	42,319	13,541	104°	chimney	2	ccw	8,5	bdg	>1	S
70	Poggio Picenze	42,32	13,542	103°	chimney	2	cw	8,5	bdg	>1	S
71	Prato Lonaro	42,276	13,364	180°	chimney	1	cw	7	bdg	1	R
72	Prato Lonaro	42,276	13,364	180°	chimney	1	cw	7	bdg	1	R
73	S. Rufina	42,331	13,353	193°	chimney	1	ccw	8	bdg	>1	S
74	S. Rufina	42,331	13,354	193°	chimney	1	cw	8	bdg	>1	S
75	S. Rufina	42,33	13,354	193°	chimney	3	ccw	8	bdg	>1	S

76	S. Eusanio (cemet.)	42,286	13,523	118°	capital	1	ccw	9	ffd	>1	S
77	S. Eusanio (cemet.)	42,287	13,523	118°	cross	1	cw	9	bdg	>1	S
78	S. Eusanio (cemet.)	42,287	13,523	118°	cross	1	cw	9	bdg	>1	S
79	S. Eusanio (cemet.)	42,287	13,523	118°	cross	1	cw	9	bdg	>1	S
80	S. Eusanio	42,288	13,524	117°	chimney	1	cw	9	bdg	>1	S
81	S. Gregorio (cemet.)	42,333	13,49	102°	pinnacle	1	cw	9	ffd	1	R
82	S. Gregorio	42,327	13,496	103°	chimney	1	ccw	9	bdg	>1	S
83	S. Gregorio	42,327	13,497	103°	chimney	1	cw	9	bdg	1	S
84	S. Pio	42,283	13,651	108°	pillar	1	ccw	5,5	ffd	>1	S
85	S. Benedetto in Bagno	42,303	13,44	126°	chimney	1	ccw	7,5	bdg	>1	S
86	S. Demetrio	42,292	13,57	111°	column	1	ccw	6,5	bdg	>1	S
87	S. Demetrio (cemet.)	42,277	13,554	116°	cross	1	ccw	6,5	ffd	>1	S
88	S. Demetrio (cemet.)	42,278	13,554	116°	cross	1	cw	6,5	ffd	>1	S
89	S. Demetrio (cemet.)	42,277	13,554	116°	monument	3	ccw	6,5	ffd	>1	S
90	S. Demetrio	42,286	13,561	114°	chimney	1	cw	6,5	bdg	>1	S
91	S. Martino d'Ocre	42,273	13,477	131°	chimney	2	cw	7	bdg	>1	R
92	S. Stefano Sessanio	42,343	13,645	92°	chimney	2	cw	6,5	bdg	1	R
93	Tempera	42,367	13,458	79°	chimney	1	ccw	9	bdg	>1	S
94	Torre de' Passeri	42,244	13,933	103°	chimney	4	ccw	6	bdg	NA	S

95	Vallecupa	42,253	13,574	122°	vase	3	NA	7,5	bdg	>1	S
96	Vallecupa	42,254	13,575	122°	statue	3	cw	7,5	ffd	>1	S
ì97	Vallecupa	42,252	13,575	122°	chimney	2	ccw	7,5	bdg	>1	S
98	Villa S. Angelo	42,27	13,538	122°	chimney	1	ccw	9	bdg	>1	S
99	Villa S. Angelo	42,27	13,538	122°	chimney	1	cw	9	bdg	>1	S
100	Villa S. Angelo	42,27	13,537	122°	chimney	2	cw	9	bdg	>1	S
101	Villa S. Angelo	42,269	13,533	124°	chimney	1	ccw	9	bdg	>1	S
102	Villa S. Angelo (cemet.)	42,265	13,536	124°	tombstone	1	cw	9	ffd	>1	S
103	Villa S. Angelo (cemet.)	42,265	13,536	124°	monument	1	ccw	9	ffd	>1	S
104	Villa S. Angelo (cemet.)	42,265	13,536	124°	gravestone	1	ccw	9	ffd	>1	S
105	Villa S. Angelo (cemet.)	42,265	13,536	124°	pillar	1	ccw	9	ffd	>1	S

Table 1 – Dataset of the rotational effects observed following the 2009 l'Aquila earthquake. AZIM is the azimuth of the site from the epicenter. The quality factor QF can vary between 1 (clearly discernible rotation) to 4 (discarded data). REMARKS: cw – clockwise, ccw – counter clockwise. MCS intensity from Galli et al., (2009). BASE: ffd – free-field based, bdg – building based. The amplification factor AF can be either 1 (stable site) or >1 (site prone to amplification). LIT: R – rigid lithology, S – soft lithology. NA: not available.

Table

	DATA (103 observations)	*NO DATA (33 observations)*
Lithology ‘R’	total 19 (18%) ffd 2 bdg 17	20 (61%)
Lithology ‘S’	total 84 (82%) ffd 35 bdg 49	13 (39%)
AF=1	total 18 (17%) ffd 2 bdg 16	16 (48%)
AF>1	total 85 (83%) ffd 35 bdg 50	17 (52%)

Table 2 – Results of the comparison between observed rotational motions and geological factors (lithology and amplification factor AF). Column ‘DATA’ refers to the dataset of rotations and reports the total number of observations along with the sub-total of the two classes of free-field based (ffd) and building based (bdg) objects (see main text and cfr. Table 1). Column ‘NO DATA’ refers to sites where rotational effects did not occur.

Table

	DATA (103 observations)	*NO DATA (33 observations)*
Cirella on fault	total 74 (72%) ffd 31 bdg 43	18 (54%)
Cirella off fault	total 29 (28%) ffd 7 bdg 22	15 (46%)
Cirella slip >0.4 m	30 (41% of the on fault, 29% of the total) ffd 16 bdg 14	7 (39% of the on fault, 21% of the total)
Atzori on fault	total 61 (59%) ffd 25 bdg 36	10 (30%)
Atzori off fault	total 42 (41%) ffd 12 bdg 30	23 (70%)
Atzori slip >0.4 m	29 (48% of the on fault, 28% of the total) ffd 16 bdg 13	3 (30% of the on fault, 9% of the total)

Table 3 – Results of the comparison between observed rotational motions and slip distribution. Column ‘DATA’ refers to the dataset of rotations and reports the total number of observations along with the sub-total of the two classes of free-field based (ffd) and building based (bdg) objects (see main text and cfr. Table 1). Column ‘NO DATA’ refers to sites where rotational effects did not occur.

Figure
Click here to download high resolution image

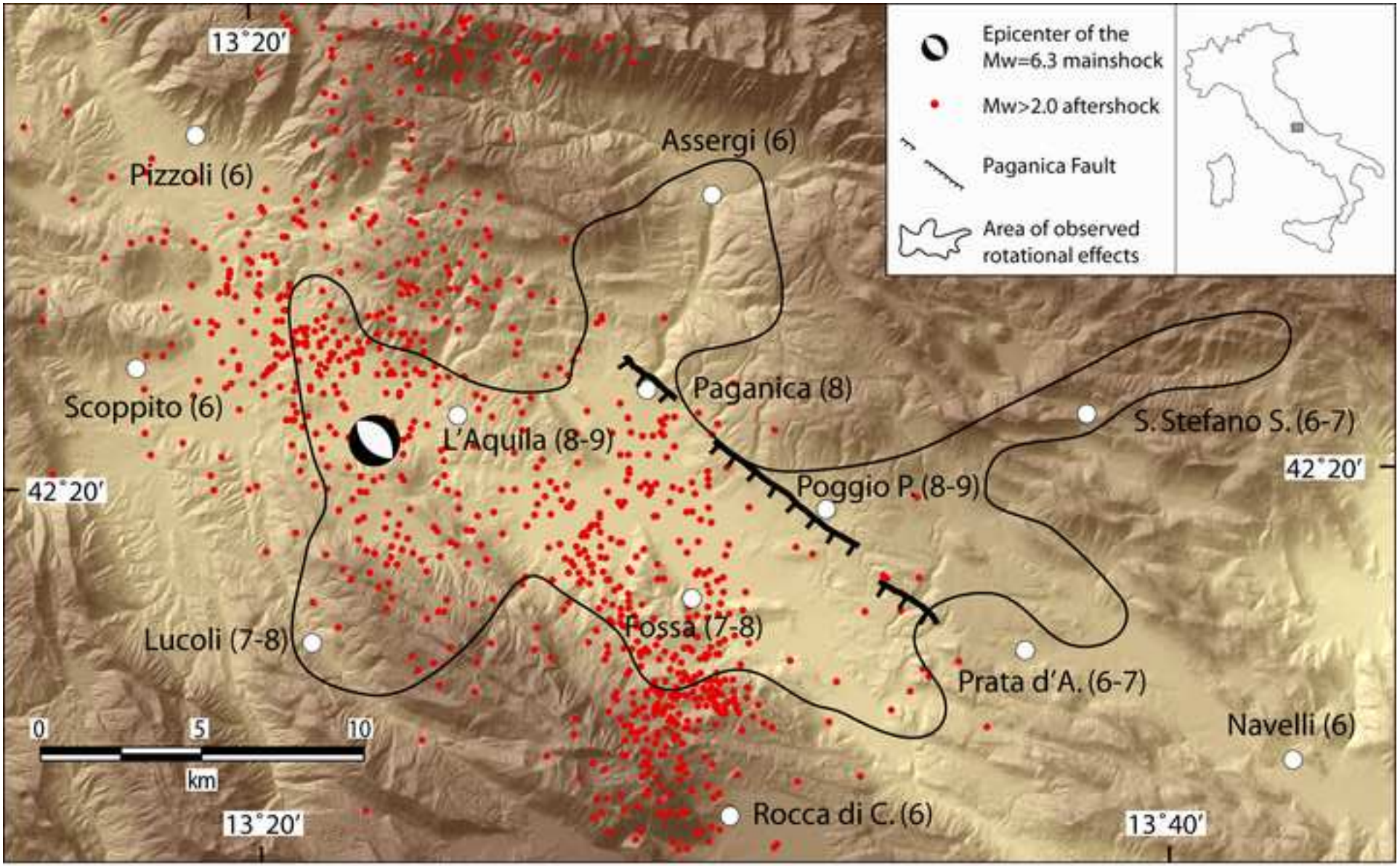

Figure 1

Figure

Click here to download high resolution image

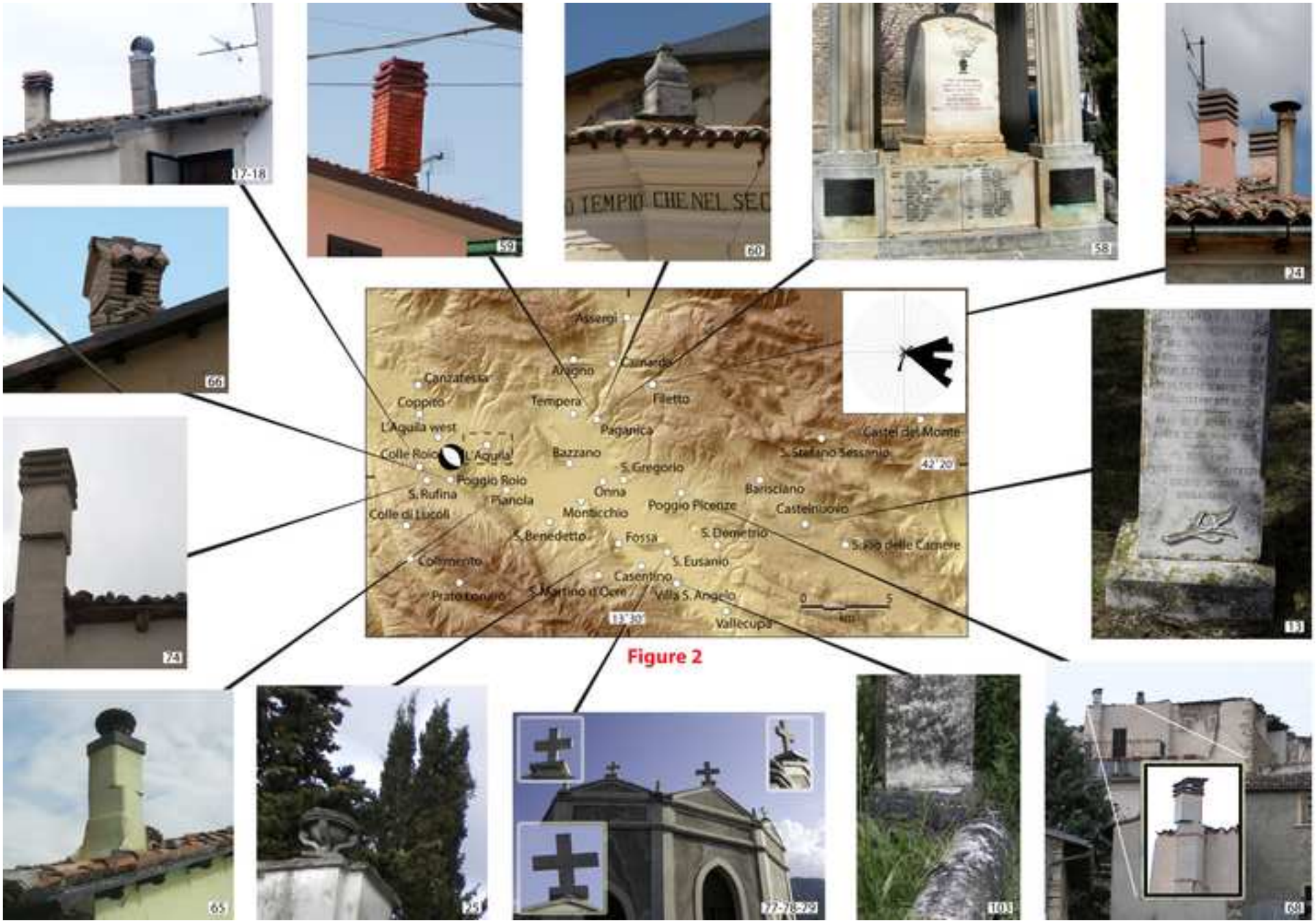

Figure
Click here to download high resolution image

Figure 3

Figure

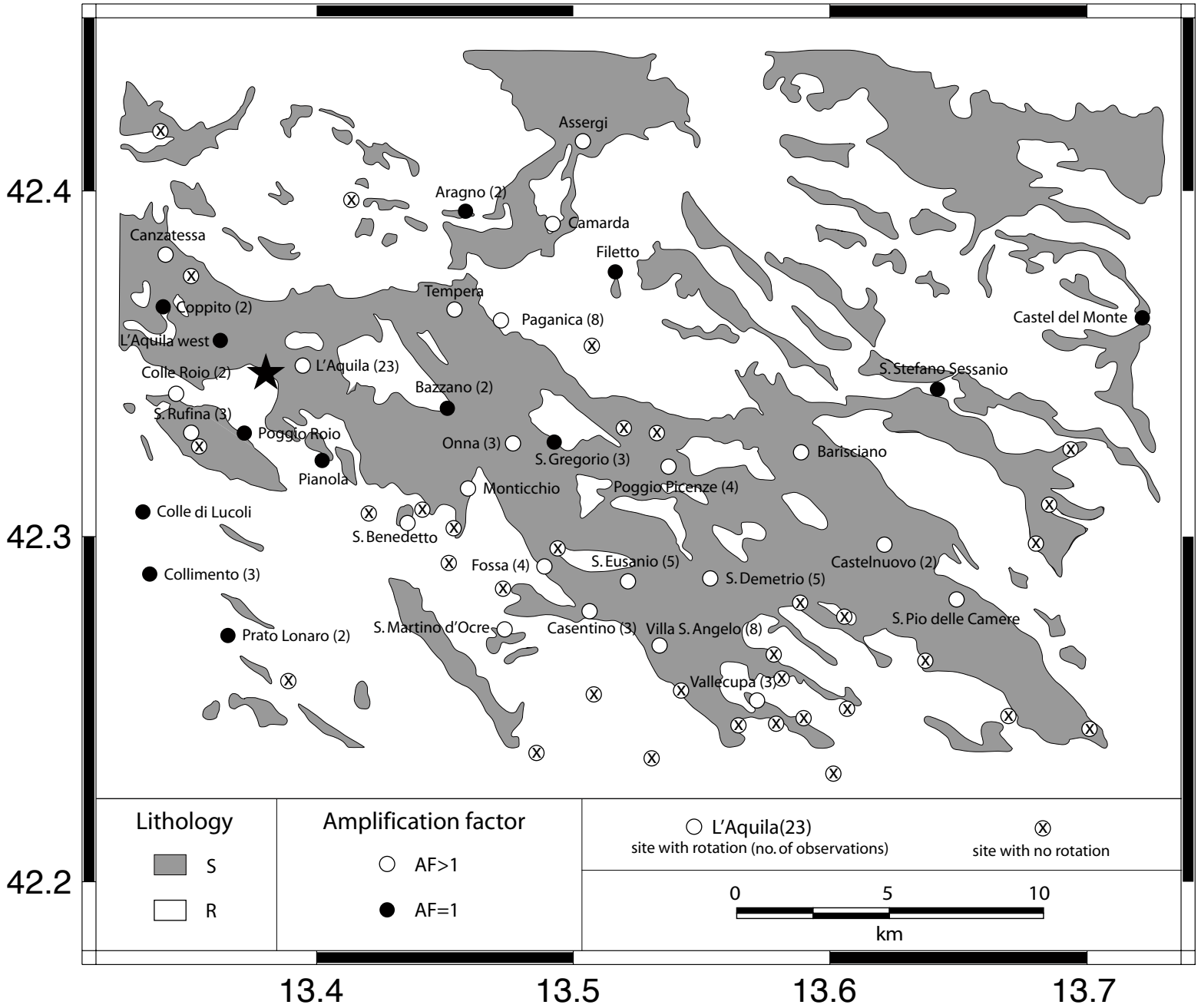

Figure 4

Figure

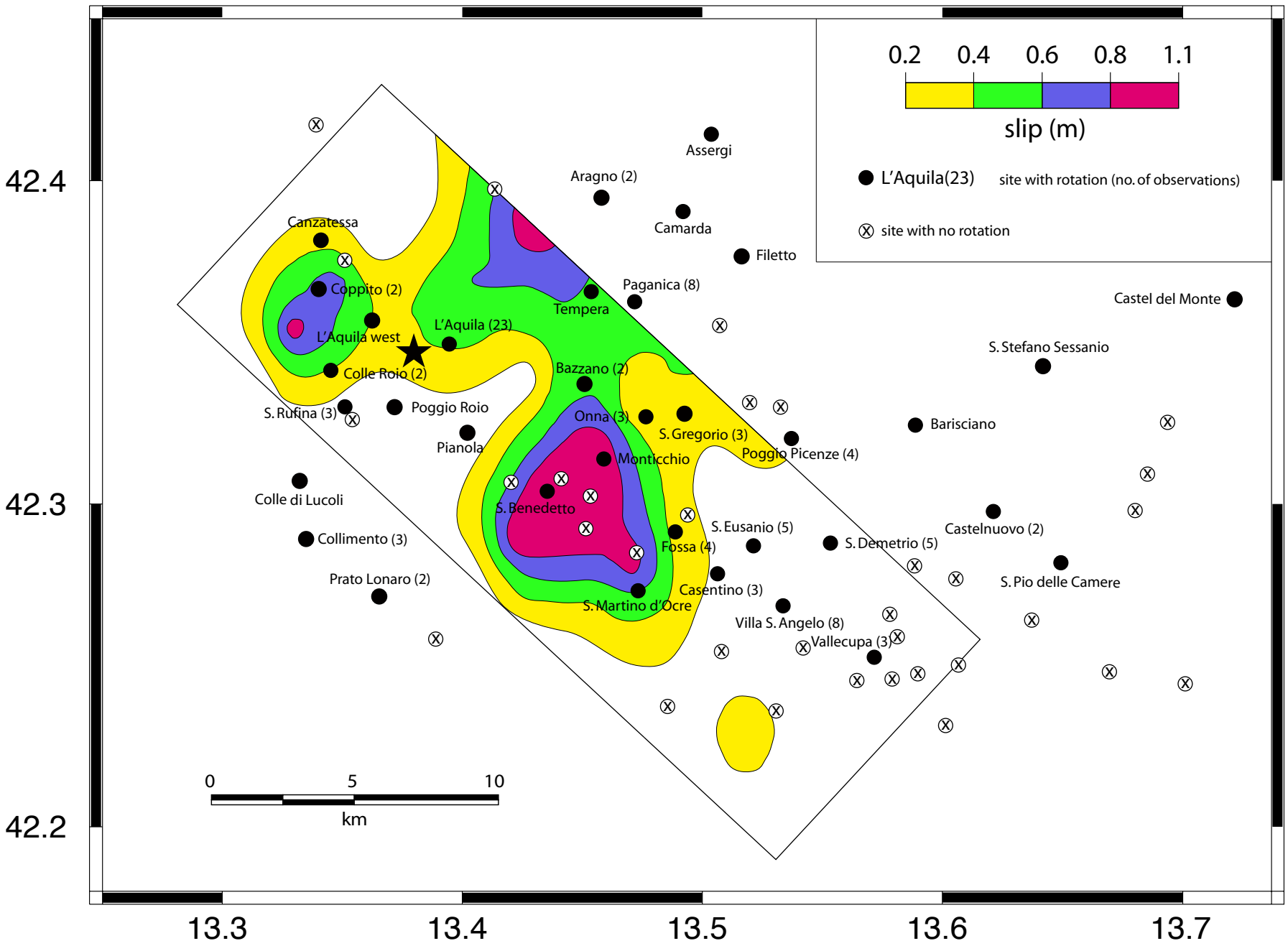

Figure 5a

Figure 5b